Journal of Electroceramics, 15, 193–202, 2005

Defects and Transport in Langasite II: Donor-doped ($La_3Ga_{4.75}Nb_{0.25}SiO_{14}$)

HUANKIAT SEH & HARRY L. TULLER

Crystal Physics and Electroceramics Laboratory, Department of Materials Science and Engineering, Massachusetts Institute of Technology, Cambridge MA 02139, USA

Submitted April 8, 2005; Revised June 8, 2005; Accepted June 9, 2005

Abstract. The electrical conductivity of Nb doped langasite ($La_3Ga_{4.75}Nb_{0.25}SiO_{14}$) was examined as a function of temperature and oxygen partial pressure by complex impedance spectroscopy. A pO_2-independent regime was found at high pO_2 followed by a $pO_2^{-1/6}$ dependent regime at low pO_2. A defect model consistent with these results was derived in which the electron density n is fixed by the density of ionized Nb donors at high pO_2 and by the generation of oxygen vacancies at low pO_2. The temperature and oxygen partial pressure dependence of the electron density was obtained independently by thermoelectric power measurements. The Nb donor ionization energy was determined to be 1.52 ± 0.06 eV, confirming Nb to be a deep donor in langasite. By combining conductivity and thermoelectric power data, an expression for the electron mobility given by $\mu_e = 1.1 \times 10^{-2} \exp(-\frac{0.15 \pm 0.01eV}{kT})$ was obtained. After evaluating the temperature dependent conductivity data under reducing conditions, in light of the defect model, a value for the reduction enthalpy ($E_r = 6.57 \pm 0.24$ eV) was derived.

Keywords: resonator, defect equilibria, electrical properties, mixed ionic-electronic conductor

Introduction

Langasite, which retains its piezoelectric properties to elevated temperatures, has operated as a surface acoustic wave device to temperatures as high as 1000°C [1], greatly surpassing the temperature limitations of other piezoelectric materials [2]. The high temperature capabilities of langasite, for example, make it a prime candidate as a crystal microbalance-based sensor for e.g. *in-situ* monitoring of automobile exhaust [3–5]. This not only requires that langasite retain its piezoelectric properties to high temperatures, but that it also remain stable in atmospheres ranging from highly reducing to oxidizing. In addition to chemical stability, electrical and mechanical losses must be minimized to prevent loss of sensor resolution and hence sensitivity [6]. Consequently, the ability to characterize and ultimately predict the electrical behavior and transport properties of langasite at elevated temperature, and over a wide oxygen partial pressure range, is crucial. In a previous paper [7], the electrical properties of acceptor-doped langasite were examined as functions of oxygen partial pressure (pO_2) and temperature and a defect model was proposed based on oxygen vacancies formed in response to acceptor dopants. The model allowed for the derivation of a series of key thermodynamic and kinetic parameters describing defect generation and transport in langasite. In this paper, donor-doped langasite ($La_3Ga_{4.75}Nb_{0.25}SiO_{14}$) is examined by both complex impedance spectroscopy and thermoelectric power measurements and a corresponding defect and transport model is derived allowing for the derivation of the Nb ionization energy, the reduction enthalpy and the electron mobility.

Theory

Acceptor-doped langasite was found to be a mixed ionic-electronic conductor with negatively charged acceptors (A') charge compensated by doubly positively charged oxygen vacancies ($V_O^{\bullet\bullet}$), rendering the oxygen vacancy the dominant ionic species and electrons and holes, minority species [7]. A defect chemical model

for acceptor doped langasite which included reduction, oxidation, electron-hole generation and acceptor-oxygen vacancy association reactions was established and confirmed [7]. The intrinsic defect generation reactions and their corresponding mass action relations are repeated here for convenience:

Anion Frenkel pair generation

$$O_O^X \rightarrow V_O^{\bullet\bullet} + O_i^{''} \tag{1}$$

$$K_F = [V_O^{\bullet\bullet}\mathbf{I}O_i^{''}] = k_F \exp\left(\frac{-E_F}{kT}\right) \tag{2}$$

Electron-hole generation

$$null \rightarrow h^{\bullet} + e^{'} \tag{3}$$

$$K_e = np = k_e \exp\left(\frac{-E_g}{kT}\right) \tag{4}$$

Reduction reaction

$$O_O^X \rightarrow V_O^{\bullet\bullet} + 2e^{'} + \frac{1}{2}O_2 \tag{5}$$

$$K_r = [V_O^{\bullet\bullet}]n^2 pO_2^{\frac{1}{2}} = k_r \exp\left(\frac{-E_r}{kT}\right) \tag{6}$$

Oxidation reaction

$$\tfrac{1}{2}O_2 + V_O^{\bullet\bullet} \rightarrow O_O^x + 2h^{\bullet} \tag{7}$$

$$K_O = p^2[V_O^{\bullet\bullet}]^{-1} pO_2^{-\frac{1}{2}} = k_O \exp\left(\frac{-E_O}{kT}\right) \tag{8}$$

For donor doped material, one includes the donor ionization reaction together with its mass action relationship:

$$D^x \rightarrow D^{\bullet} + e^{'} \tag{9}$$

$$K_{Dn} = [D^{\bullet}]n/[D^x] = k_{Dn} \exp\left(\frac{-E_{D\_ion}}{kT}\right) \tag{10}$$

in which D^x and $D^{\bullet}$ represent unionized and ionized donors respectively, and k_{Dn} is simply the conduction band density of states N_c (in cm^3). Further, one applies the donor mass conservation relationship given by:

$$[D_{\text{total}}] = [D^x] + [D^{\bullet}] \tag{11}$$

Finally, the general electrical neutrality equation, incorporating all the above defect species, can be written as:

$$n + 2[O_i^{''}] = p + 2[V_O^{\bullet\bullet}] + [D^{\bullet}] \tag{12}$$

In cases of restricted pO_2 range and temperature, the Brouwer approximation can be applied to simplify the neutrality equation so as to include only one defect specie on each side of the equality sign. Commonly, for donor-doped materials, four defect regions are defined: reduction, ionic compensation, electronic compensation, and oxidation. In each region, the neutrality equation, Eq. (12), is simplified and by substitution into the above equations, allows one to readily solve the set of simultaneous defect equations (Eqs. (2), (4), (6), (8), (10)–(12)) for the listed defects as functions of oxygen partial pressure and temperature. The solutions are summarized in Table 1 and the corresponding Kroger-Vink diagram, schematically illustrates the characteristic pO_2 dependences of the listed defect species in Fig. 1.

For cases where the measured electrical response spans over more than one defect region, the Brouwer approximation is inexact. For example, as we demonstrate below, the electrical conductivity straddles regions Region II at high pO_2, and Region I at low pO_2. In this case, a neutrality equation, inclusive of all major defect species, must be used:

$$[D^{\bullet}] + 2[V_O^{\bullet\bullet}] = n \tag{13}$$

By substituting Eq. (13) into Eq. (6) and solving for n, one obtains the cubic equation:

$$n^3 - [D^{\bullet}]n^2 - 2pO_2^{-\frac{1}{2}}k_r \exp\left(-\frac{E_r}{kT}\right) = 0 \tag{14}$$

which can be solved to obtain a closed form solution for n.

To solve for n in Eq. (14), appropriate approximations for $[D^{\bullet}]$ need to be made. At high or intermediate pO_2, where the degree of reduction remains limited, Eq. (13) can be approximated by $[D^{\bullet}] \approx n$. Substituting into Eq. (10) and solving for n:

$$n = [D^{\bullet}] = [D^X]^{\frac{1}{2}} k_{Dn}^{\frac{1}{2}} \exp\left(-\frac{E_{D\_ion}}{2kT}\right) \tag{15}$$

Table 1. Equations for defect species concentration in donor doped material.

Electrical carrier	Region I $n \approx 2\left[V_O^{\bullet\bullet}\right]$	Region II $n \approx [D_c^{\bullet}]$	Region III $2[O_i^{''}] \approx [D_c^{\bullet}]$	Region IV $p \approx 2[O_i^{''}]$
n	$2^{\frac{1}{3}} pO_2^{-\frac{1}{6}} k_r^{\frac{1}{3}} \exp\left(\frac{-E_r}{3kT}\right)$	$[D^{\bullet}] = [D^X]^{\frac{1}{2}} k_{Dn}^{\frac{1}{2}} \exp\left(-\frac{E_{ion}}{2kT}\right)$	$2^{\frac{1}{2}} [D_c^{\bullet}]^{-\frac{1}{2}} pO_2^{-\frac{1}{4}} k_r^{\frac{1}{2}} k_F^{\frac{1}{2}} \exp\left(-\frac{(E_r+E_F)}{2kT}\right)$	$2^{\frac{1}{3}} pO_2^{-\frac{1}{6}} k_o^{-\frac{1}{3}} k_e \exp\left(-\frac{\left(E_g - \frac{1}{3}E_o\right)}{kT}\right)$
p	$2^{-\frac{1}{3}} pO_2^{+\frac{1}{6}} k_r^{-\frac{1}{3}} k_e \exp\left(-\frac{(E_g - \frac{1}{3}E_r)}{kT}\right)$	$[D_c^{\bullet}]^{-1} k_e \exp\left(-\frac{E_g}{kT}\right)$	$2^{-\frac{1}{2}} [D_c^{\bullet}]^{\frac{1}{2}} pO_2^{\frac{1}{4}} k_r^{-\frac{1}{2}} k_F^{-\frac{1}{2}} k_e \exp\left(\frac{(E_r+E_F-2E_g)}{2kT}\right)$	$2^{-\frac{1}{3}} pO_2^{\frac{1}{6}} k_o^{\frac{1}{3}} \exp\left(-\frac{E_o}{3kT}\right)$
$[V_O^{\bullet\bullet}]$	$2^{-\frac{2}{3}} pO_2^{-\frac{1}{6}} k_r^{\frac{1}{3}} \exp\left(\frac{-E_r}{3kT}\right)$	$[D_c^{\bullet}]^{-2} pO_2^{-\frac{1}{2}} k_r \exp\left(-\frac{E_r}{kT}\right)$	$2[D_c^{\bullet}]^{-1} k_F \exp\left(-\frac{E_F}{kT}\right)$	$2^{\frac{2}{3}} pO_2^{-\frac{1}{6}} k_o^{-\frac{1}{3}} k_F^{\frac{2}{3}} \exp\left(-\frac{\left(2E_F - E_o\right)}{3kT}\right)$
$[O_i^{''}]$	$2^{\frac{2}{3}} pO_2^{+\frac{1}{6}} k_r^{-\frac{1}{3}} k_F \exp\left(-\frac{(E_F - \frac{1}{3}E_r)}{kT}\right)$	$[D_c^{\bullet}]^2 pO_2^{\frac{1}{2}} k_r^{-1} k_F \exp\left(-\frac{(E_F - E_r)}{kT}\right)$	$\frac{1}{2}[D_c^{\bullet}] = \frac{[D_c^x]}{2n} k_{Dn} \exp\left(-\frac{E_{D\_ion}}{kT}\right)$	$2^{-\frac{2}{3}} pO_2^{\frac{1}{6}} k_o^{\frac{1}{3}} k_F^{\frac{1}{3}} \exp\left(-\frac{(E_F+E_o)}{3kT}\right)$

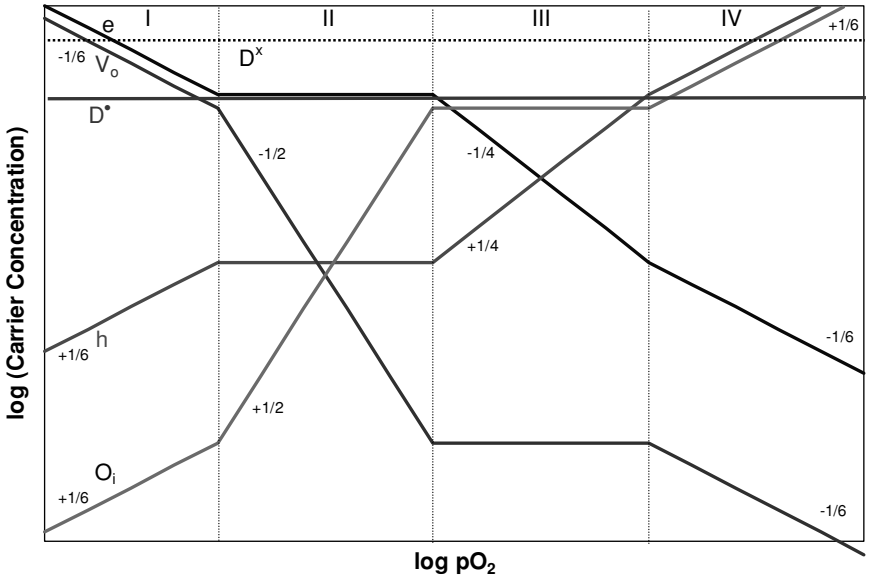

Fig. 1. Kroger-Vink diagram for donor doped material.

Note, this assumes that D is a deep donor and is only partially ionized. As demonstrated below, this assumption holds true for Nb in langasite even for elevated temperatures. Furthermore, in this regime where n is fixed by the ionized donor density, n is predicted to be independent of pO_2. If the electron mobility is activated, the conductivity activation energy in this regime will be the sum of half the donor ionization energy and the electron migration (mobility activation) energy, i.e.:

$$E = 1/2 \quad E_{D\_ion} + E_\mu \tag{16}$$

At sufficiently low pO_2, Eq. (13) is approximated by $n \approx 2[V_O^{\bullet\bullet}]$. Substituting into Eq. (6) and solving for n:

$$n = (2k_r)^{\frac{1}{3}} \exp\left(\frac{-E_r}{3kT}\right) pO_2^{-\frac{1}{6}} \tag{17}$$

In order to isolate the contributions of carrier ionization and migration, thermoelectric power (TEP) measurements were initiated permitting the determination of the concentration and type of electronic species [8, 9]. The TEP (or Seebeck coefficient Q) represents the slope of the voltage induced across a specimen upon imposition of a temperature gradient. Since carriers diffuse down the thermal gradient, the polarity of the contact at the cool end reflects the charge of the dominant electronic species. For an n-type semiconductor, n is related to Q by [10]:

$$Q = -\frac{k}{e}\left[\ln\frac{N_C}{n} + \frac{H_e^*}{kT}\right] \tag{18}$$

in which N_c is the conduction band density of states and H_e^* is the heat of transport, all other terms have their usual meaning. In semiconducting oxides, the heat of transport, H^*, is typically small and usually neglected [11]. By combining information about the electron concentration from Q and the electron conductivity data from the impedance measurements, it becomes possible to extract values for the electron mobility, i.e. $\mu_e = (\sigma_e/ne)$.

Experimental

Sample Preparation

Polycrystalline langasite samples with 5% of Ga substituted by Nb ($La_3Ga_{4.75}Nb_{0.25}SiO_{14}$) were produced using the mixed oxide route. Proportional amount of La_2O_3, Ga_2O_3, SiO_2 and Nb_2O_5 powders (Alfa Aesar, 99.99% metal basis) were mixed and ball milled in water for a day. The mixture was then dried at 110°C while stirred, and then uniaxially pressed into 1" pellets. The

pellets were calcined at 950°C for 3 hours and then sintered at 1450°C for 10 hours and a density of greater than 90% was achieved. X-ray diffraction showed that there was no observable second phase. The pellets were then cut into 2 × 2 mm cross sectional sample bars using a die-saw. Platinum electrodes, used for electrical measurements, were painted on using platinum paint from Engelhard-Clal and then sintered at 850°C for 3 hours.

Bulk Electrical Conductivity

Two-point impedance measurements, using a Solartron 1260 Impedance Analyzer, were performed on the Nb-doped langasite sample under a range of controlled temperatures and oxygen partial pressures. The temperature was controlled within a tube furnace and the pO_2 was varied by using CO/CO_2 or O_2/Ar gas mixtures. Samples were allowed to equilibrate from a day (at 700°C) to 2hr (at 1000°C). Tests for reversibility were performed by repeating measurements at higher pO_2 after measurements had been completed at low pO_2.

The bulk electrical conductivity was determined at each temperature and pO_2 by fitting the corresponding impedance spectrum with an equivalent circuit that contained a number of parallel R-C elements in series, one each for electrodes, grain boundaries and bulk. From the value of bulk resistance, the bulk conductivity of the material was calculated after normalizing for the specimen geometry.

Thermoelectric Power (TEP) Measurement

In order to determine the electron concentration in donor-doped langasite, TEP measurements were performed as a function of pO_2 and temperature. The schematic of the experimental setup is shown in Fig. 2. The donor-doped langasite sample was a bar about 15 mm long, with a pair of type-S thermocouples on each end to record the temperature (using thermometer, Omega HH506R) differential along the sample. The temperature gradient was generated simply by moving the sample along the furnace axis. The voltage between the two thermocouples was recorded using a Keithley 197 nanovoltmeter, after allowing the sample to equilibrate for about an hour between each set of conditions.

Concentration Cell Measurements

The experimental apparatus for obtaining values for the ionic transport number t_i, the fractional ionic conductivity, $t_i = \sigma_i/\sigma_{\text{total}}$, is described in detail in a previous paper [7]. Briefly, a pO_2 gradient is imposed across the specimen and the open circuit emf thereby induced is measured as a function of pO_2. Ionic conductors will exhibit the Nernst potential, while specimens exhibiting largely electronic conductivity will exhibit a nearly zero open circuit potential. As we see below, Nb doped langasite, in contrast to acceptor doped langasite, exhibits no measurable ionic conductivity.

Results

The bulk electrical conductivity of 5%Nb-doped langasite is plotted as function of pO_2 and temperature in Fig. 3. The conductivity is observed to be pO_2 independent at high pO_2 but becomes successively more pO_2 sensitive at reduced pO_2 approaching an approximately $pO_2^{-\frac{1}{6}}$ dependence under the most reducing conditions.

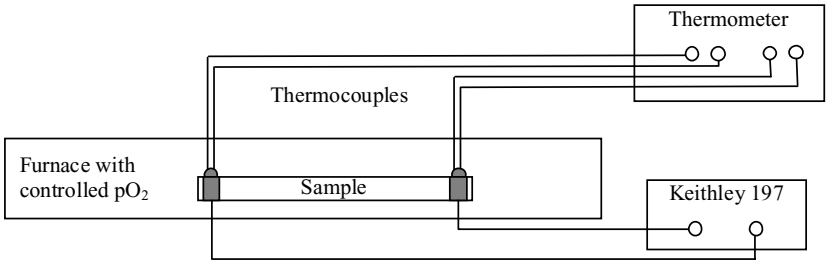

Fig. 2. Experimental setup for thermoelectric power measurements.

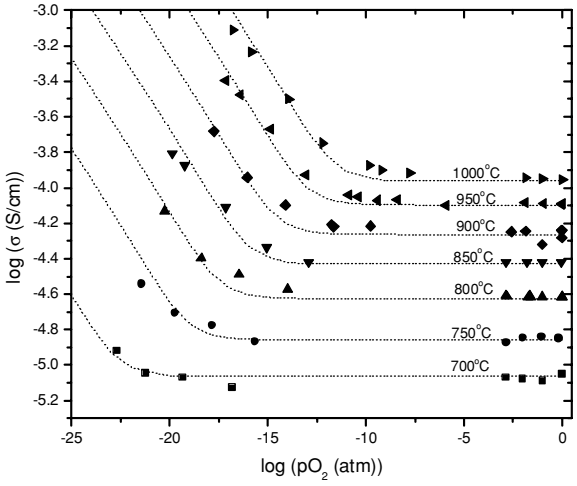

Fig. 3. Bulk electrical conductivity of 5% Nb-doped langasite. The symbols.

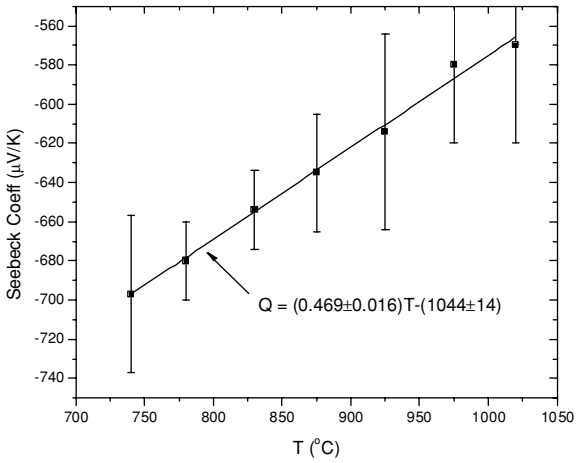

Fig. 5. TEP or Seebeck coefficients of 5% Nb-doped langasite in air as a function of temperature.

In the oxygen independent regime (high to intermediate pO_2), the activation energy for conduction should, according to Eqs. (15) and (16), be related to the sum of the donor ionization and electron migration energies. The pO_2-independent electrical conductivity is plotted as a function of reciprocal temperature in Fig. 4 for which one calculates an activation energy of 0.91 ± 0.01 eV. In order to deconvolute the two energetic contributions, TEP measurements were performed. The Seebeck coefficient, Q, measured in air as a function of temperature, is shown plotted in Fig. 5. The electron density, n, derived with the aid of Eq. (18), is shown plotted in Fig. 6 as a function of reciprocal temperature. The calculated activation energy of 0.76 ± 0.03eV, represents, according to Eq. (15), half the donor ionization energy. The fact that n is thermally activated also confirms that the Nb level is not a shallow but rather a deep donor level. By combining the electron density and conductivity data from the

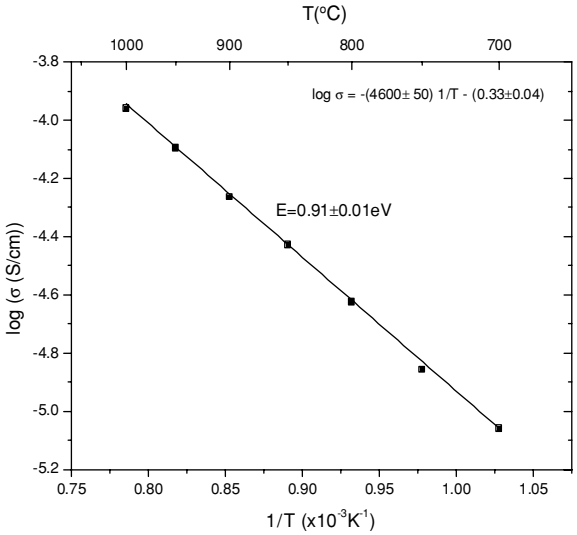

Fig. 4. Temperature dependence of the pO_2-independent conductivity.

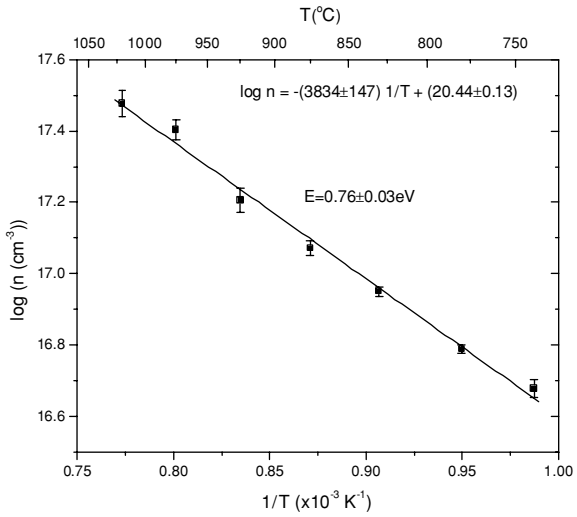

Fig. 6. Electron density of 5% Nb-doped langasite in air as function of temperature.

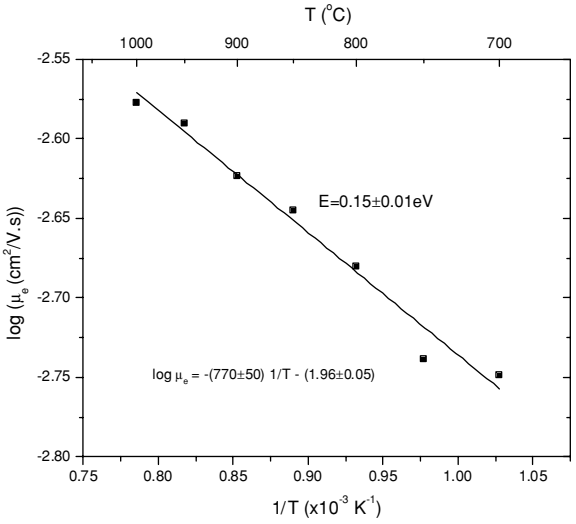

Fig. 7. Electron mobility as function of temperature.

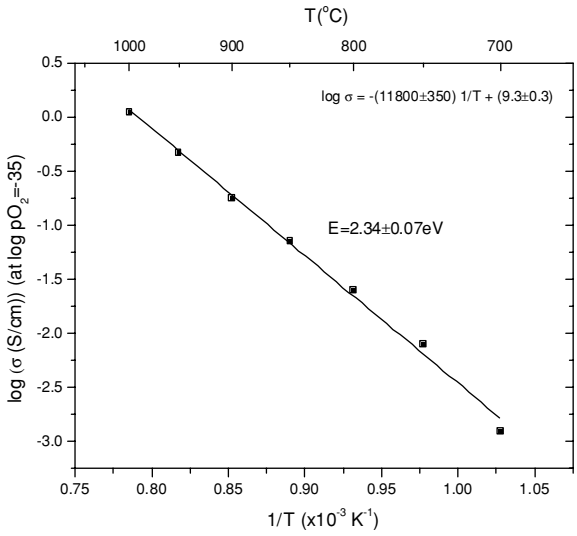

Fig. 8. pO_2 dependent electronic conductivity extrapolated to $pO_2 = 10^{-35}$atm.

pO_2-independent regime, the electron mobility, ($\mu_e = \sigma_e/nq$), is obtained as function of temperature. Note that the actual data for both electron density and conductivity are used, not the fitted results. The results, plotted in Fig. 7, show the electron mobility, μ_e, to be temperature-dependent with an activation energy of 0.15 ± 0.01 eV.

Next, we examine the pO_2 dependent electronic conductivity under reducing conditions. The increasing magnitude of the conductivity with reducing pO_2 points to n-type conductivity, as confirmed by the sign of Q. By extrapolating the electrical conductivity using a $pO_2^{-\frac{1}{6}}$-dependence to very low pO_2, e.g. $pO_2 = 10^{-35}$ atm, the activation energy for the highly reducing regime can be obtained by plotting the conductivity at fixed pO_2 as a function of inverse temperature (Fig. 8). The activation energy is found to be 2.34 ± 0.07 eV.

The Seebeck coefficient Q, measured as function of pO_2 at 950°C, is shown plotted in Fig. 9. The corresponding electron density, calculated with the aid of Eq. (18), is shown plotted in Fig. 10 also as a function of pO_2. Also shown are values of the electron density derived from the corresponding conductivity data (dotted curve in Fig. 3) assuming a value for the electron mobility as derived previously in Fig. 7. The excellent agreement between the two sets of data demonstrates that the calculated electron mobility is insensitive to changes in pO_2 and can be used, in combination with the measured conductivity data, to estimate the electron density at any temperature or pO_2.

Finally, the open circuit voltage, measured across Nb doped langasite-based concentration cells, was found to be on the order of mV even under large pO_2 gradients rather than the order of hundreds of millivolts as expected for ionic conductors (see Fig. 11). These measurements, therefore, confirm that the conductivity

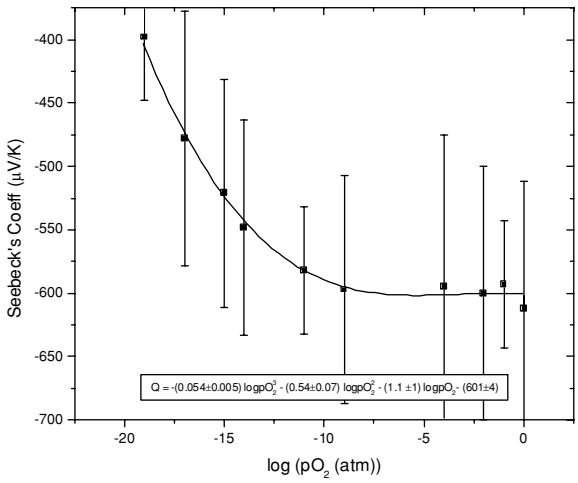

Fig. 9. TEP or Seebeck coefficient of 5% Nb-doped langasite at 950°C as a unction of pO_2.

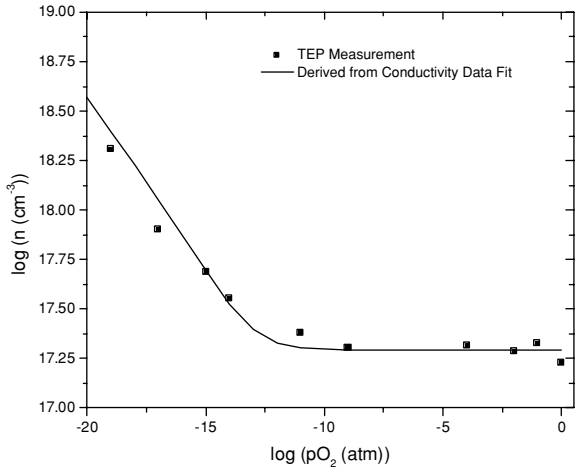

Fig. 10. Electron density of 5% Nb-doped langasite at 950°C as a function of pO_2. The symbols represent n values derived from the TEP data collected over a wide range of pO_2 The solid curve is the electron density calculated from conductivity measurements.

of Nb doped langasite is predominantly electronic at all accessible temperatures and pO_2's.

Discussion

The bulk electrical conductivity data of 5%Nb-doped langasite, together with the TEP and concentration cell measurements, enable us to apply a defect model in explaining the electrical transport properties of donor-doped langasite. As briefly discussed in the introduction, the conductivity data for 5%Nb-doped langasite is predominantly electronic. The dominant electronic conductivity is confirmed by concentration cell measurements.

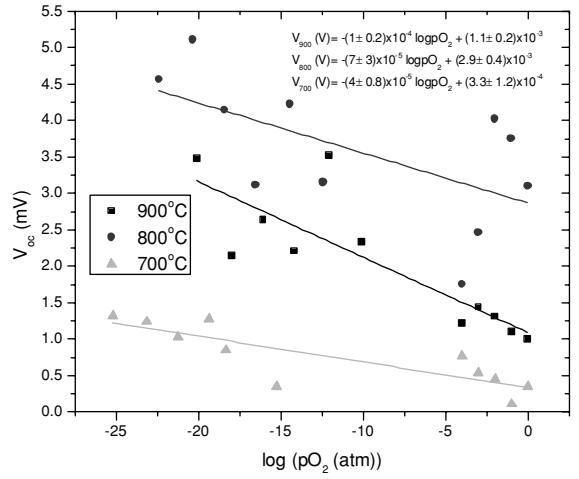

Fig. 11. V_{oc} versus pO_2 concentration cell data for 5% Nb-doped langasite.

The activation energy for conduction in the pO_2-independent regime was found to be 0.91 ± 0.01 eV (Fig. 4). Given the high activation energy, it was deemed highly unlikely that the electron migration energy would be the sole contributor to that activation energy. Alternatively, given a deep donor level, and therefore only partial ionization, then the activation energy represents the sum of electron migration energy and half the donor ionization energy. This hypothesis was confirmed by the TEP results which demonstrated that n ($n \approx [D^{\cdot}]$) was indeed a strong function of temperature even in the pO_2 plateau region (Fig. 6).

The activation energy of 0.76 ± 0.03 eV, as obtained for n, represents, according to Eq. (15), half the donor ionization energy. Therefore, the donor ionization energy is given by 1.52 ± 0.06 eV, confirming Nb to be a deep donor in langasite. Next, the migration energy, utilizing Eq. (16), is calculated to be 0.15 ± 0.01 eV, a value commonly associated with small polaron hopping, as is the magnitude of $\mu_e \approx 2 \times 10^{-3}$ cm^2/V-sec for the temperature range of 700–1000°C [12]. Furthermore, the electron mobility was shown to be independent of pO_2, as commonly assumed for non-stoichiometric oxides [9].

The y-intercept value for Fig. 6 corresponds to $\log([D^X]^{\frac{1}{2}} k_{Dn}^{\frac{1}{2}})$ (see Eq. (15)):

$$\log([D^X]^{\frac{1}{2}} k_{Dn}^{\frac{1}{2}}) = 20.44 \tag{19}$$

As observed in Fig. 6, only a small fraction of the total donor ($[\mathrm{Nb_{total}}] = 8.5 \times 10^{20} \mathrm{cm}^{-3}$) is ionized, and therefore Eq. (11) can be rewritten as an approximation:

$$[D_{\mathrm{total}}] \approx [D^x] \tag{20}$$

As k_{Dn} is simply N_c, this allows us to calculate for N_c using Eq. (19) and (20):

$$k_{Dn} = N_c = 8.9 \times 10^{19} \quad cm^{-3} \tag{21}$$

Next, turning to the $pO_2^{-\frac{1}{6}}$-dependent regime, the activation energy for electron generation in this regime should, according to Eq. (17), represent one third of the reduction enthalpy. For the activation energy for conduction, one must add the electron migration energy of 0.15 ± 0.01 eV. Given a measured activation energy of conductivity of 2.34 ± 0.07 eV, the reduction enthalpy for La-doped langasite is calculated to be 6.57 ± 0.24 eV, approximately 0.9 eV larger than the value of 5.7 $\pm$ 0.06 eV obtained for acceptor-doped langasite [7]. Such differences are not unexpected given that the 5% Nb additive would certainly be expected to induce a deviation from the dilute solution approximation. Similar changes in reduction enthalpy were observed by Tuller and Nowick for CeO_2 in which the addition of 5 mol% Y_2O_3 (acceptor) in solid solution induced a decrease in the reduction enthalpy of undoped ceria from 4.7 eV to 4.0 eV [11].

According to Eq. (17), given knowledge of $n(T,pO_2)$, it becomes possible to obtain an expression for K_r. For example, by normalizing the conductivity data in Fig. 8 by the electron mobility, one obtains $n(T,\ pO_2\ = 10^{-35} atm)$. Following this approach, K_r was calculated and is plotted in Fig. 13. As expected from the above discussion, the activation energy for K_r is 6.57 ± 0.24 eV, identical to the result calculated above ($E_r = 6.57 \pm 0.24$ eV).

It is instructive to examine how the equilibrium constant data can be used to predict the pO_2 at a given temperature for which the electron density n shifts from donor control, $[D^{\bullet}] \approx n$, to reduction control, $n \approx 2[V_O^{\bullet\bullet}]$. The transition pO_2 is defined by the condition in Fig. 12 for which the contributions to conductivity from the reduction reaction and donors become equal. Therefore by equating Eq's (15) and (17), one obtains:

$$2^{\frac{1}{3}} pO_{2,\text{transition}}^{-\frac{1}{6}} k_r^{\frac{1}{3}} \exp\left(\frac{-E_r}{3kT}\right) = [D^x]^{\frac{1}{2}} k_{Dn}^{\frac{1}{2}} \exp\left(\frac{-E_{D\_ion}}{2kT}\right) \quad (22)$$

Rearranging:

$$\log pO_{2,\text{transition}} = -\frac{2E_r - 3E_{D\_ion}}{kT \log e} + \log\left(4[D^x]^{-3} k_{Dn}^{-3} k_r^2\right) \quad (23)$$

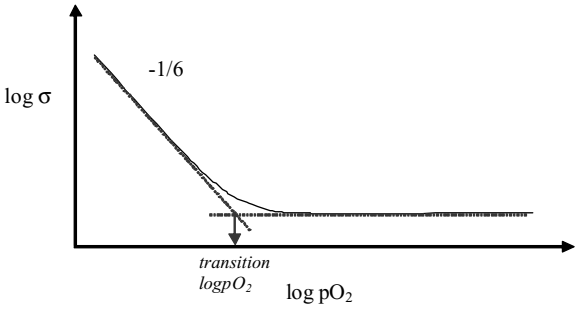

Fig. 12. Definition of transition pO_2 for donor doped material.

The transition pO_2's were estimated from Fig. 3 and are plotted in Fig. 14 as a function of reciprocal temperature. The derived activation energy from the plot is 8.62 ($\pm$ 0.38) eV, which should correspond to $2E_r$-$3E_{D\_ion}$. As calculated previously, $E_r = 6.57(\pm 0.24)$ eV (donor-doped) and $E_{D\_ion} = 1.52(\pm 0.06)$ eV, giving the value of $8.64(\pm 0.66)$ eV for $2E_r$-$3E_{D\_ion}$, in excellent agreement with the identical value derived from the data in Fig. 14.

Table 2 summarizes the results obtained for the thermodynamic and kinetic parameters derived for Nb doped langasite. These constants, when coupled with the defect chemical model presented in this report, provide the means for predicting the concentrations of electrons and oxygen vacancies as a function of tem-

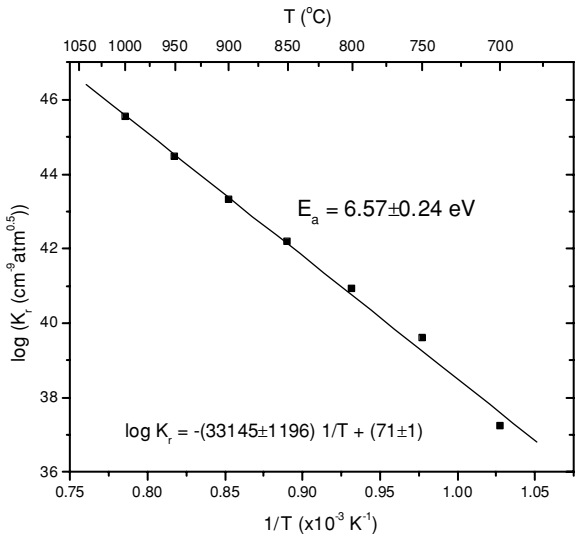

Fig. 13. K_r as function of temperature for langasite.

Table 2. Summary of results.

	Donor-doped Langasite
K_r $(cm^{-9}atm^{0.5})$	$K_r = 10^{71} \exp\left(-\frac{6.57 \pm 0.24eV}{kT}\right)$
Nb Ionization (cm^{-3})	$[Nb^{\bullet}] = 2.75 \times 10^{20} \exp\left(-\frac{1.52 \pm 0.06eV}{2kT}\right)$
$\mu_e(cm^2/Vs)$	$\mu_e = 1.1 \times 10^{-2} \exp\left(-\frac{0.15 \pm 0.01eV}{kT}\right)$

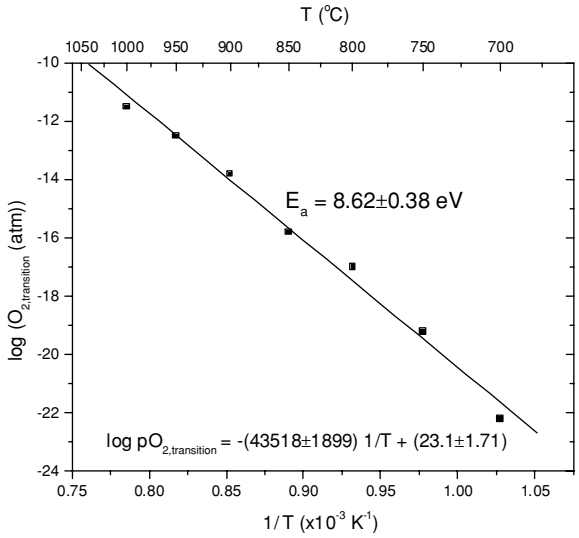

Fig. 14. Transition pO_2 (see definition in text) versus reciprocal temperature for 5 % Nb-doped langasite.

perature and pO_2 for donor doped langasite. Furthermore, with the expression for the electron mobility, the bulk conductivity can be predicted as function of dopant concentration, temperatures and pO_2. The dotted curves in Fig. 3 were calculated in this manner.

Conclusion

The transport properties of Nb doped langasite were investigated using complex impedance, concentration cell and thermoelectric power measurements. A defect model was developed and used to describe the electrical properties as functions of temperature, dopant level and pO_2. This model provides a framework for explaining the observed transport properties and the underlying physical processes.

The conductivity was found to be *n*-type electronic at all examined temperatures and pO_2's, as confirmed by thermoelectric power and concentration cell measurements. The electrons dominated the conductivity, leading to a donor compensated regime at high pO_2 and a reduction dominated regime at low pO_2. Nb was found to be a deep donor with ionization energy of 1.52 ± 0.06 eV, as confirmed by thermoelectric power measurements. The electron mobility of langasite was found to be activated (small polaron hopping) with an activation energy of 0.15 ± 0.01 eV. Using the defect model, the reduction enthalpy for donor doped langasite was determined to be 6.57 ± 0.24 eV.

Acknowledgment

We thank the National Science Foundation (NSF DMR-9701699, DMR-0228787 and INT-9910012) for the support that made this work possible. The authors also thank H. Fritze for his on going collaboration on the subject of langasite.

References

1. J.W. Mrosk, C. Ettl, L. Berger, P. Dabala, H.J. Fecht, G. Fischerauer, J. Hornsteiner, K. Riek, E. Riha, E. Born, W. Werner, A. Dommann, J. Auersperg, E. Kieselstein, B. Michel, and A. Mucha, in *Proceedings of 24th Annual Meeting of IEEE Industrial Electronics Society*, IECON 1998, 1998: p. 2386–2390.
2. D. Damjanovic, *Current Opinion in Solid State & Materials Science*, **3**, 469 (1998).
3. R. Mital, J. Li, S.C. Huang, B.J. Stroia, and R.C. Yu, SAE Technical Paper Series (2003-01-0041), 2003.
4. M.S. Brogan, A.D. Clark, and R.J. Brisley, *Recent progress in NOx trap technology.* SAE Technical Paper Series (980933), 1998.
5. Y.-W. Kim, J. Sun, I. Kolmanovsky, and J. Koncsol, *A phenomenological control oriented lean NOx trap model.* SAE Technical Paper Series (2003-01-1164), 2003.
6. H. Fritze, H.L. Tuller, H. Seh, and G. Borchardt, *Sensors and Actuators B*, **76**, 103 (2001).
7. H. Seh and H.L. Tuller, *Accepted by Journal of Electroceramics*, for publication.
8. W.D. Kingery, H.K. Bowen, and D.R. Uhlmann, *Introduction to Ceramics*. John Wailey & Son 1976.
9. D.M. Smyth, *The Defect Chemistry of Metal Oxides*., Oxford University Press (2000).
10. H.L. Tuller, *Mixed conduction in nonstoichiometric oxides*, in *Nonstoichiometric Oxides*, O.T. Sorensen, (Academic Press, New York). (1981) p. 271–335.
11. H.L. Tuller and A.S. Nowick, *Journal of Electrochemical Society*, **126**(2), 209 (1979).
12. H.L. Tuller and A.S. Nowick, *Journal of Physics and Chemistry of Solids.,* **38**, 859 (1977).